Journal of Structural Geology 32 (2010) 1887–1898

Contents lists available at ScienceDirect

Journal of Structural Geology

journal homepage: www.elsevier.com/locate/jsg

Multiple causes of diagenetic fabric anisotropy in weakly consolidated mud, Nankai accretionary prism, IODP Expedition 316

Kitty L. Milliken*, Robert M. Reed

Bureau of Economic Geology, Jackson School of Geosciences, The University of Texas at Austin, 10100 Burnet Road, Austin, TX 78713, USA

ARTICLE INFO

Article history:
Received 4 August 2009
Received in revised form
23 February 2010
Accepted 17 March 2010
Available online 2 June 2010

Keywords:
Mud
Mudrock
Mudrock fabric
Compaction
Diagenesis

ABSTRACT

In the Nankai accretionary prism and its associated slope sediments early (pre-lithification) mechanical modification of mud induces preferred alignments of elongate or platy particles and the loss of intergranular porosity. Generic types of particle alignment include: 1. particles having long axes aligned in the plane of bedding, most likely as a consequence of burial compaction; 2. diverse bioturbation structures including alignments parallel to burrow walls, burrows filled with obliquely aligned phyllosilicates, and blotchy disruption of bedding; and, 3. planar deformation bands showing parallel alignments of both silt- and clay-size particles.

Subtle compositional contrast between deformation bands and host rocks is consistent with loss of intergranular micropores within bands and supports the dominance of mechanical over chemical processes in their formation. Field-emission SEM imaging of Ar-ion-milled cross-sections shows that collapse of larger (>2 μm) pores, many localized at the margins of silt-size particles, reduces porosity within the bands by about 5 percent compared to the adjacent host rock. Despite the clear role of shear, evidence for particle comminution is equivocal.

These observations on mechanical processes in early diagenesis provide useful context for interpretation of pore types and fabric anisotropies in mudrocks across a wide range of subsurface conditions.

1. Introduction

In accretionary prisms gravity-driven mass transport and compressional tectonic stresses interact with burial compaction early in the post-depositional history to impart macro- and micro-scale fabric anisotropies in mud (Karig and Lundberg, 1990; Prior and Behrmann, 1990; Behrmann and Kopf, 1993; Maltman, 1998; Ujiie et al., 2004). The presence of deformational fabrics in the shallow regions of accretionary prisms is of great interest because, owing to low geothermal gradients and resultant low temperatures, these complex early diagenetic mechanical processes can be readily examined without a strong overprint of thermally-driven chemical processes. At the same time, the combination of structural loading and high sedimentation rates in the prism environment yields samples of relative compositional uniformity that can be sampled across a broad range of depths. Thus, the accretionary prism setting is an excellent natural laboratory for examining early mechanical processes in mud.

Diagenesis is defined as inclusive of chemical and mechanical processes that affect sediments in the subsurface following deposition and prior to the onset of metamorphism or weathering (Milliken, 2003). Historically, however, much of the literature on post-depositional sediment alteration has focused on chemical processes within a conceptual framework that assumes an absence of deformation. Recent technical innovations for micro-scale imaging have fostered a growing recognition of a wide array of pervasive deformation features in rocks having very simple structural histories (e.g., Milliken, 1994; Laubach, 1997; Milliken and Laubach, 2000). *Structural diagenesis* (see Laubach et al., 2010 this issue) focuses attention on chemical and mechanical processes that affect structures on all scales in sedimentary rocks prior to the onset of metamorphism, emphasizing a more rigorous application of mechanics principles for understanding rock fabrics, even in little-deformed rocks, while also emphasizing the impact of chemical processes on the evolution of rock mechanical properties. Very importantly, this conceptual framework highlights the important genetic linkages that apply in some cases amongst chemical and mechanical processes in sedimentary basins.

This study focuses on a case in which the mechanical processes of diagenesis dominate over chemical processes in the modification of

* Corresponding author. Tel.: +1 512 471 6082; fax: +1 512 471 0140.
E-mail address: kitty.milliken@beg.utexas.edu (K.L. Milliken).

0191-8141/$ – see front matter © 2010 Elsevier Ltd. All rights reserved.
doi:10.1016/j.jsg.2010.03.008

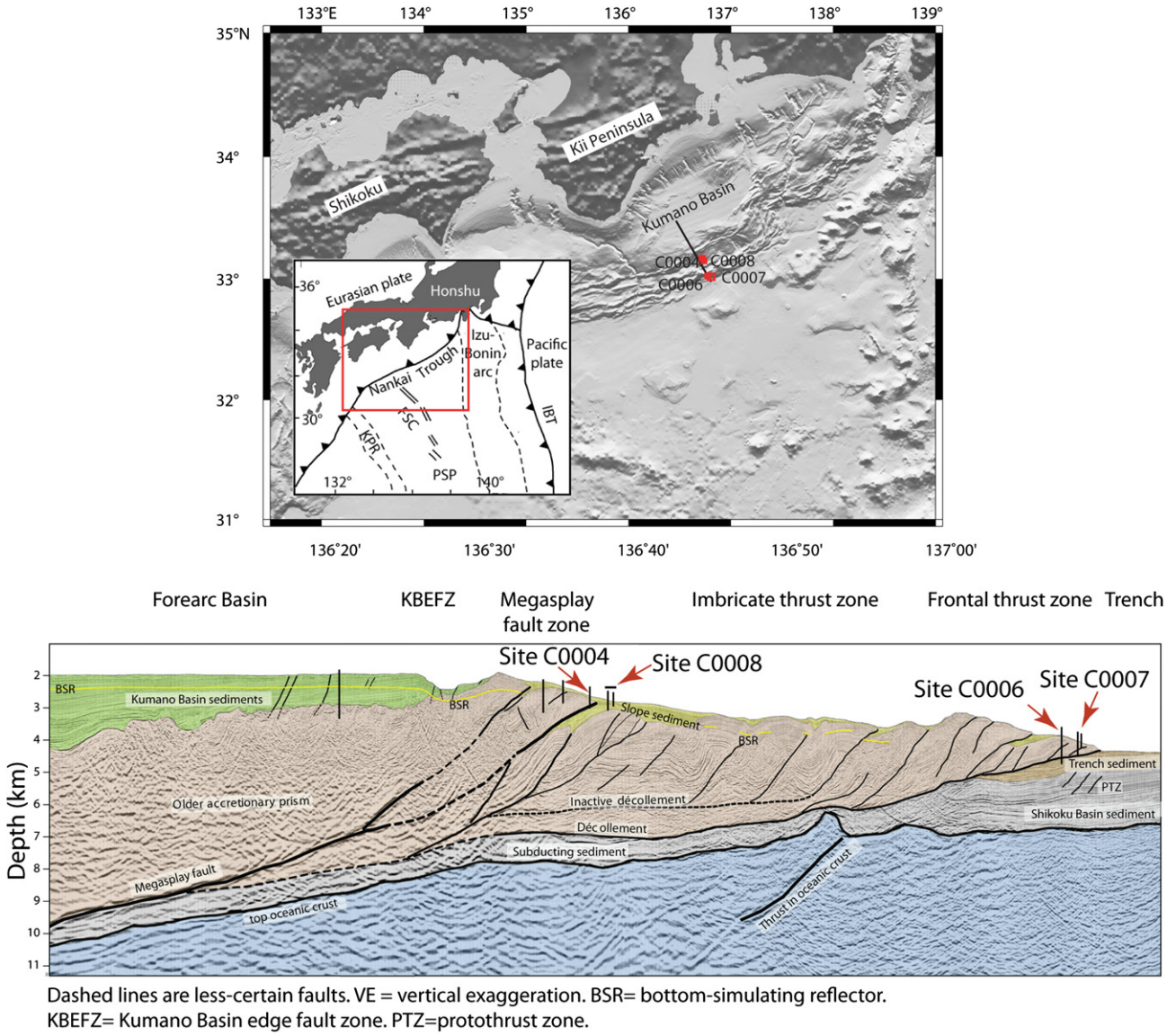

Fig. 1. A. Bathymetry and locations of Sites C0004, C0008, C0006, and C0007, part of a transect of sites drilled off the Kii Peninsula during Stage 1 of the NanTroSEIZE project. Modified from Moore et al. (2009) and Screaton et al., (2009). B. Interpreted structure cross-section showing the locations of drill sites C0004 and C0008 in the vicinity of the mega-splay and Sites C0006 and C0007 near the toe of the prism. Modified from Moore et al. (2009), their Fig. 6.

rock fabric and properties. Direct observation using a variety of micro-scale imaging techniques supports suggestions of previous studies concerning the dominant roles of porosity loss and particle reorientation and the lesser roles of particle comminution and chemical modification in the evolution of early diagenetic fabric anisotropy in mud. Fabric anisotropies and deformation localization documented here are clearly affiliated with embryonic stages in the diagenetic history and provide useful context for interpretation of similar features that may be observed in mudrocks that have experienced a more protracted history of deep burial and, especially, heating that may induce chemical processes such as cementation. This preliminary study reports, in part, results of our experimentation with imaging and analysis protocols that are useful for quantitative characterization of mudrock fabric and pore systems at the micro-scale.

2. Sampling and methods

Pleistocene and Pliocene mud samples were obtained at IODP Sites C0004, C0006, C0007, and C0008 during IODP Expedition 316 (Kinoshita et al., 2009; Screaton et al., 2009) (Fig. 1; Table 1). Site C0004 is slightly landward of the mega-splay fault whereas Site C0008 is located at a small slope basin seaward of the intersection of the mega-splay with the sea floor (Strasser et al., 2009). Sites C0006 and C0007 are near the toe of the accretionary prism. Hemipelagic muds for this study range in burial depth from near the modern sediment surface to a depth of 573 (mbsf) and were obtained routinely, in concert with sampling of turbidite sands for provenance study, one or two samples per core, without regard to specific associations with macroscopically visible deformational features, thus providing an essentially random sampling of mudrock fabrics-Intervals rich in nannofossils and ash layers were avoided; samples described here are dominated by extrabasinal siliciclastic debris. Texturally, samples are dominantly silt-bearing clay-rich mudstone (classification of Macquaker and Adams, 2003), but range into sand- and silt-bearing clay-rich mudstone, and clay-rich mudstone (Fig. 2). Considerable textural heterogeneity is present within some individual thin sections as seen in Fig. 2D. All of the samples this study are weakly consolidated and

can be readily disaggregated into their natural particles by placing them in distilled water and applying moderate sonication.

Thin sections of 82 samples were cut perpendicular to bedding, but no attempt was made to orient the samples other than to preserve the bedding direction and in some cases, the up-direction. Thin sections were ground to standard thickness (30 μm). Vacuum-pressure epoxy impregnation is not effective in these very low-permeability muds so surface impregnation using a low-viscosity medium was employed to reduce plucking and to preserve rock fabric during the final polish of the sections. Thin sections were observed in transmitted and reflected polarized light under both plane-light and cross-polarization. A full-wave plate (gypsum plate) was used in transmitted cross-polar observation to accentuate the spatial variations in the orientation of the phyllosilicate components. This method highlights, through visible changes in the amplified birefringence during stage rotation, the overall orientation, in aggregate, of particles that are too small to see individually.

Back-scattered electron (BSE) imaging and X-ray mapping by wavelength dispersive spectroscopy (WDS) was performed on a JEOL 8200 Super probe. Mapping runs used either 0.5 or 1 μm stage increments, a 40 ms count time, and a 50 nA sample current (as measured on brass), and a focused spot (~1 μm). Texture and fabric (silt content, particle size, particle shape, particle orientation) within the bands and adjacent host rocks were analyzed from BSE images (1000x original magnification) using the image analysis program JMicrovision (Roduit, 2008). Images were displayed on a tracing screen and all particles >2 μm (9 Phi units; silt/clay boundary) were digitally traced and established as 2D objects for determination of equivalent circular diameter and other measures of particle size, shape, and orientation. For two samples data from 3 such images were combined for each determination; data for the third sample is based one image for the band and on one for the host rock.

Thin sections or rock slabs smoothed by mechanical polishing cannot be used to make reliable observations of natural porosity in mudrocks, first, because average mudrock pores are much smaller than the thickness of a standard thin section, and second, because of ambiguities arising from artificial pores created by mechanical damage that occurs during polishing (Loucks et al., 2009). To overcome these problems, pore observations made by secondary electron imaging on a Zeiss Supra field-emission scanning electron microscope (FE-SEM) using cross-section surfaces prepared utilizing a Gatan Ar-ion-mill (Loucks et al., 2009). Material for milling was trimmed from the unimpregnated central portion of the thin section blank, thus allowing some correlation of observations to be made across the various petrographic methods. The sample imaged for this study was milled at 5.0 kV and 350 μA for ~48 h and then coated with Ir. An irregular surface of ~1.3 mm^2 was created, measuring approximately 4.3 mm long and 0.54 mm wide at its widest. Pores >2 μm apparent diameter were point-counted using JMicrovision for regions within the band and host rocks (750 points each) from an image mosaic obtained at an initial magnification of 1350x.

3. Results of particle alignment and rock fabric analysis

Table 2 summarizes the distribution of three manifestations of detrital phyllosilicate alignment across the sample set. "Phyllosilicate" here refers to clay minerals in the clay-size (<2 μm) fraction as well as to detrital micas and chlorite that occur both in the silt fraction and the upper range of the clay-size fraction. Samples that lack either bedding-parallel or bioturbation-related phyllosilicate alignments (i.e., have apparently random alignments) are rare. Nearly *all* samples display bedding-parallel phyllosilicate alignment, bioturbation-related particle alignments, or both. Deformation bands are also widely distributed and are somewhat more abundant near the toe of the prism (60% of samples at Sites C0006 and C0007) than in the region of the mega-splay (43% of samples at Sites C0004 and C0008).

3.1. Bed-parallel alignment

The most common form of phyllosilicate alignment is parallel in the plane of the bedding (Fig. 3) and is generally uniform across the sample. The intensity of bedding-parallel alignment varies with the silt content, generally being more pronounced in more clay-rich samples, consistent with the observations of previous studies (Curtis et al., 1980; Oertel, 1983; Day-Stirrat et al., 2010) that admixture of equant sand- or silt-size particles reduces the intensity of clay alignment.

3.2. Biogenically induced alignment

Phyllosilicate alignments related to biogenic structures show great variability between samples and also at the thin section scale (Fig. 4). Many samples display blotchy disruptions of the more uniform bedding-parallel alignment, leading to a variety of very irregular textures that lack the distinct shapes and sharp walls of burrows (Fig. 4A). Another form of spatially localized preferred alignment is seen in clay-filled burrows in which the internal clay filling has a prominent preferred alignment that contrasts markedly with the alignment in the surrounding mud (Fig. 4B, C). Some tubular burrows have walls with a pronounced tangential arrangement of phyllosilicates (Fig. 4D).

3.3. Planar deformation structures (deformation bands)

Planar deformation structures constitute the third class of preferred alignments observed in these mudstones. The importance of shear in the development of these localized structures is evidenced by markers of apparent strain such as offsets of features such as foraminifer tests and pyrite-filled and clay-filled burrows (Fig. 5). Most planar shear bands intersect the sample at a high angle to bedding although a few are bed-parallel. The smallest discernible bands are in the range of a few microns across (Fig. 6). Smaller bands tend to have a simple planar form while some larger ones form complex anastomosing patterns that envelope volumes of undeformed mud between undulose zones of shear containing strongly aligned phyllosilicates (Fig. 7).

Back-scattered electron images reveal the bands as distinct zones of higher BSE brightness, with edges that are sharp at the scale of a few microns (Fig. 8). No particular mineral phase can be identified as a cause for the increased BSE intensity. X-ray maps of bands and adjacent host rocks (Fig. 8) reveal an overall higher Si-content within the bands, but no systematic increase in Fe, K, Na, or Ca.

Contrast in particle size between bands and adjacent host rocks is variable (Table 3). The most consistent difference is a diminished content of the larger particles within the bands. Only one of three samples examined (C0006E-27X-8, 6 cm) shows a consistently finer population across most of the size range (Fig. 9). Bands generally display a fractal dimension (D in Table 3) somewhat higher than host rocks, consistent with a degree of particle comminution within bands. Contrasting particle alignment in bands and host rocks in two of the three samples examined can be detected in the silt-size fraction as well as the clay-size fraction (Fig. 10, Table 3).

FE-SEM imaging of Ar-ion milled surfaces reveals readily discernible contrasts in pore systems in a deformation band and its adjacent host rock (Fig. 11). In the host rock, many of the larger pores are affiliated with margins of larger silt-size particles. Within bands these larger pores are diminished in abundance. A point-count of pores > 2 μm diameter, shows that the host rock and the

Table 1
Sample set.

Unit	age	Site-Hole-Core-Section, cm	Depth (mbsf)	thin section number (VXL)	clay-rich mudstone type	bed-parallel orientation	burrow mottles	defm bands	comments
Site C0004									
I	Pliocene	C0004C-9H-5, 71 cm	78.08	1	silt-bearing	x		x	
I	Pliocene	C0004C-9H-5, 73 cm	78.10	2	silt-bearing	x	x	x	
IIB	Pliocene	C0004D-25R-2, 23 cm	257.65	3	silt-bearing	x	x		
III	Pliocene	C0004D-27R-1, 13 cm	265.14	4	silt-bearing	x		x	brecciated
III	Pliocene	C0004D-28R-1, 8 cm	269.59	5	silt-bearing	x	x	x	brecciated
III	Pliocene	C0004D-29R-CC, 18 cm	277.14	6	silt-bearing	x	x	x	brecciated
III	Pliocene	C0004D-33R-1, 83 cm	292.84	7	silt-bearing	x	?	x	kink bands
III	Pliocene	C0004D-35R-1, 66 cm	301.67	8	silt-bearing	x	x	x	kink bands
III	Pliocene	C0004D-36R-1, 23 cm	305.74	9	silt-bearing	x	x	x	kink bands
IV	Pleistocene	C0004D-38R-CC, 16 cm	315.43	10	sand- and silt-bearing	x	?		
IV	Pleistocene	C0004D-40R-1, 57 cm	324.08	11	silt-bearing	x	x		
IV	Pleistocene	C0004D-41R-1, 22 cm	328.23	12	sand- and silt-bearing	x	x	x	
IV	Pleistocene	C0004D-42R-3, 12 cm	335.05	13	sand- and silt-bearing	x	x		
IV	Pleistocene	C0004D-44R-1, 86 cm	342.37	14	silt-bearing	x			
IV	Pleistocene	C0004D-46R-1, 78 cm	351.29	15	silt-bearing	x			
IV	Pleistocene	C0004D-48R-1, 117 cm	360.68	16	silt-bearing	x	x		
IV	Pleistocene	C0004D-50R-1, 121 cm	369.72	17	silt-bearing	x	x		
IV	Pleistocene	C0004D-52R-2, 3 cm	378.94	18	silt-bearing	x	x		
IV	Pleistocene	C0004D-53R-1, 72 cm	382.74	19	silt-bearing	x	x	x	
IV	Pleistocene	C0004D-54R-3, 133 cm	390.65	20	silt-bearing	x	x		
IV	Pleistocene	C0004D-55R-2, 57 cm	392.99	21	sand- and silt-bearing	x	x		
IV	Pleistocene	C0004D-56R-2, 90 cm	397.83	22	sand- and silt-bearing	x	x	x	
				22		22	18	11	
Site C0008									
IA	Pleistocene	C0008A-2H-7, 10 cm	14.19	69	sand- and silt-bearing	?	x		
IA	Pleistocene	C0008C-3H-4, 75 cm	18.74	70	silt-bearing	x	?		
IA	Pleistocene	C0008A-8H-3, 92 cm	66.56	71	sand- and silt-bearing		x		
IA	Pleistocene	C0008A-15H-3, 92 cm	121.40	72	silt-bearing	x	x		
IA	Pleistocene	C0008A-19H-1, 28 cm	150.18	73	silt-bearing	x	x		
IA	Pleistocene	C0008C-23X-5, 78 cm	151.44	74	silt-bearing	x	x		
IA	Pleistocene	C0008A-23H-3, 16 cm	180.52	75	silt-bearing	x	x		
IA	Pleistocene	C0008A-24H-3, 116 cm	190.16	76	silt-bearing	x	x	x	
IA	Pleistocene	C0008A-27H-1, 96 cm	211.36	77	silt-bearing	x	x	x	
IA	Plio-Pleist	C0008A-30X-1, 68 cm	234.94	78	silt-bearing	x	x		
IA	Pleistocene	C0008A-29X-7, 70 cm	231.60	79	silt-bearing	x	x	x	
IB	Plio-Pleist	C0008A-33X-7, 17 cm	269.20	80	clay-rich	x	x	?	
II	Pliocene	C0008A-34X-CC, 15 cm	272.99	81	clay-rich	x	x	x	kink bands
II	Pliocene	C0008A-38X-1, 7 cm	310.33	82	clay-rich	x	x		
				14		13	14	5	
Site C0006									
I	Pleistocene	C0006E-2H-8, 58 cm	12.92	23	silt-bearing	x	x		
I	Pleistocene	C0006E-3H-8, 38 cm	22.28	24	sand- and silt-bearing	x	x	x	
IIA	Pleistocene	C0006E-4H-6, 47 cm	30.63	25	silt-bearing	x	x		
IIB	Pleistocene	C0006E-20X-3, 50 cm	128.68	26	silt-bearing	x	x		
IIB	Pleistocene	C0006E-21X-CC, 25 cm	139.54	27	sand- and silt-bearing	x		x	
IIB	Pleistocene	C0006E-23X-7, 46 cm	161.37	28	silt-bearing	x	x	x	
IIC	Pleistocene	C0006E-26X-8, 92 cm	191.81	29	silt-bearing	x	x	x	
IIC	Pleistocene	C0006E-27X-8, 6 cm	200.39	30	silt-bearing	x	x	x	
IIC	Pleistocene	C0006E-28X-2, 95 cm	203.70	31	silt-bearing	x	x	x	bed-parallel bands
IIC	Pleistocene	C0006E-30X-4, 30 cm	223.84	32	silt-bearing	x	x	x	
IIC	Pleistocene	C0006E-32X-7, 54 cm	246.97	33	silt-bearing	x	x	x	
IIC	Pleistocene	C0006E-36X-1, 122 cm	278.56	34	silt-bearing	x	x		
IIC	Pleistocene	C0006E-38X-CC, 23 cm	297.53	35	silt-bearing	x		x	
IIC	Pleistocene	C0006E-39X-1, 129 cm	307.13	36	silt-bearing	x	x		
IIC	Pleistocene	C0006E-40X-3, 76 cm	318.93	37	silt-bearing	x	?		
IIC	Pleistocene	C0006E-43X-CC, 14 cm	352.24	38	silt-bearing	x	?	x	
IIC	Pleistocene	C0006E-44X-3, 110 cm	357.28	39	silt-bearing	x	x		
IID	Pleistocene	C0006E-48X-3, 96 cm	395.13	40	silt-bearing	x	x		
IID	Pleistocene	C0006E-49X-2, 13 cm	402.38	41	silt-bearing	x	x	x	
IID	Pleistocene	C0006F-3R-2, 52 cm	414.92	42	silt-bearing	x	x		
IID	Pleistocene	C0006F-5R-1, 69 cm	433.70	43	silt-bearing	x	x		
III	Pleist-Miocene	C0006F-11R-1, 121 cm	486.73	44	clay-rich	x	x	x	
III	Pleist-Miocene	C0006F-12R-1, 27 cm	495.28	45	clay-rich	x	x	x	
III	Pleist-Miocene	C0006F-14R-1, 111 cm	515.12	46	clay-rich	x	x		
III	Pleist-Miocene	C0006F-18R-1, 10 cm	552.13	47	silt-bearing	x	x	x	

Table 1 (*continued*)

Unit	age	Site-Hole-Core-Section, cm	Depth (mbsf)	thin section number (VXL)	clay-rich mudstone type	bed-parallel orientation	burrow mottles	defm bands	comments
III	Pleist-Miocene	C0006F-20R-2, 38 cm	572.80	48	silt-bearing	x	x	x	
				26		26	24	15	
Site C0007									
I	Pleistocene	C0007A-1H-3, 42 cm	2.10	49	sand- and silt-bearing	x	x		
I	Pleistocene	C0007C-1H-7, 58 cm	18.91	50	silt-bearing	x	x	x	
IIAi	Pleistocene	C0007C-5X-CC, 22 cm	43.42	51	sand- and silt-bearing	x	?		
IIAi	Pleistocene	C0007C-7X-1, 128 cm	63.38	52	silt-bearing	x	x		
IICi	Pleistocene	C0007D-4R-1, 14 cm	199.65	53	sand- and silt-bearing	x	x		
IICi	Pleistocene	C0007D-5R-1, 64 cm	209.65	54	silt-bearing	x	x		
IICi	Pleistocene	C0007D-7R-1, 69 cm	228.70	55	silt-bearing	x	x	x	
IICi	Pleistocene	C0007D-8R-2, 57 cm	239.49	56	silt-bearing	x	x		
IICii	Pleistocene	C0007D-16R-1, 51 cm	313.52	57	silt-bearing	x		x	
IICii	Pleistocene	C0007D-17R-1, 67 cm	323.18	58	silt-bearing	x	x	x	
IID	Pleistocene	C0007D-18R-1, 35 cm	332.37	59	silt-bearing	x	x		
IID	Pleistocene	C0007D-19R-2, 82 cm	343.74	60	silt-bearing	x	x	x	
III	Pliocene	C0007D-22R-1, 33 cm	370.34	61	silt-bearing	x	x	x	
III	Pliocene	C0007D-23R-2, 36 cm	381.28	62	silt-bearing	x	x	x	bed-parallel bands
III	Pliocene	C0007D-23R-3, 53 cm	382.88	63	silt-bearing	x	x	x	bed-parallel bands
III	Pliocene	C0007D-24R-3, 96 cm	392.82	64	silt-bearing	x	x	x	bed-parallel bands
III	Pliocene	C0007D-25R-3, 20 cm	401.58	65	clay-rich	x	x	x	
III	Pliocene	C0007D-26R-2, 23 cm	409.66	66	clay-rich	x	x	x	
III	Pliocene	C0007D-28R-3, 34 cm	430.20	67	clay-rich	x	x		
III	Pleistocene	C0007D-29R-1, 100 cm	437.52	68	clay-rich	x	x	x	
				20	20	20	19	12	

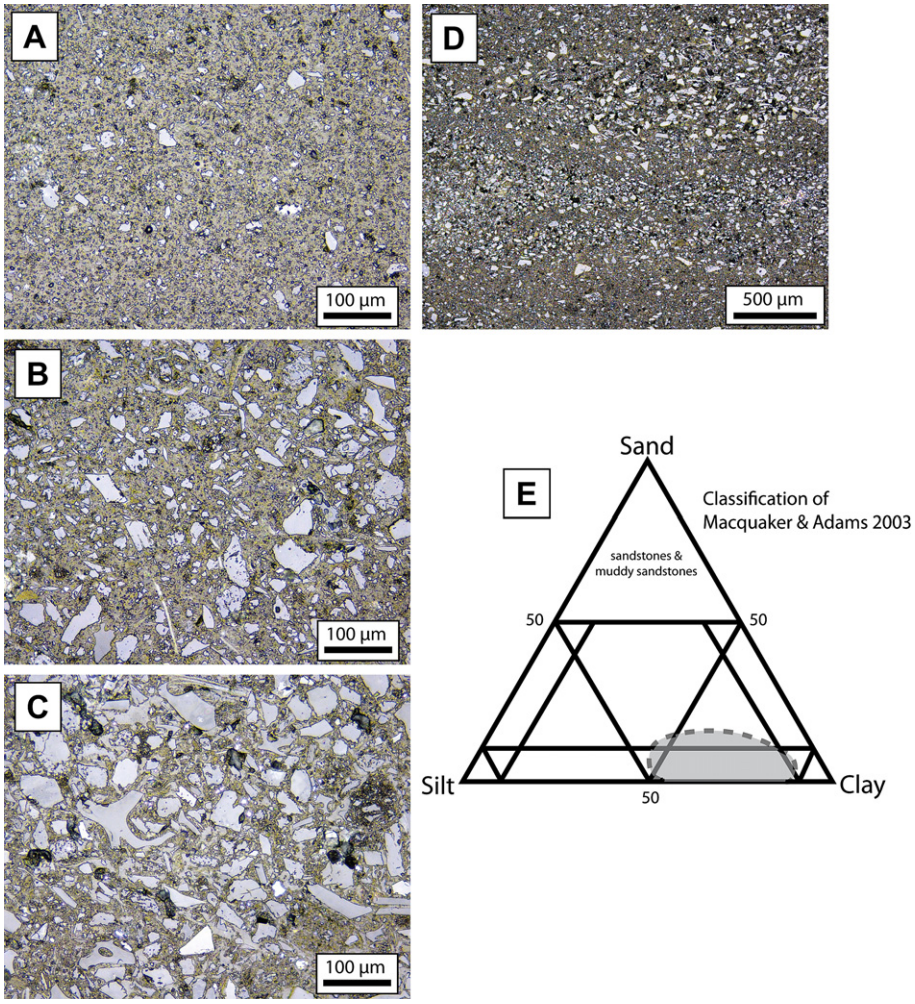

Fig. 2. Textural variations of the sampled mudstones. All in bright-field reflected light. A) Clay-rich mudstone. B) Silt-bearing clay-rich mudstone (most common type of sample). C) Sand- and silt-bearing clay-rich mudstone. D) Example of textural heterogeneity within a single thin section. E) Classification of Macquaker and Adams (2003). Textural compositions of the samples in this study fall predominantly within gray region delimited by the dashed line.

Table 2
Summary of structure occurrence.

Site	n	bed-parallel orientation (% of samples)	burrow mottles (% of samples)	defm bands (% of samples)	min depth[a] (m)
C0004	22	100	82	50	78
C0008	14	93	100	36	190
C0006	26	100	92	58	22
C0007	20	100	95	60	19
total/avgs	82	98	92	51	

[a] minimum depth at which deformation bands are observed.

adjacent band, include pore space,of 8.3 and 3.6 percent by volume, respectively. Pores smaller than 2 μm diameter cannot be reliably measured, even in this high-resolution image.

4. Discussion

An extensive body of work documents fabric anisotropy in accretionary prism sediments, both in the Nankai prism (Karig and Lundberg, 1990; Byrne et al., 1993; Maltman et al., 1993; Morgan and Karig, 1993; Lewis et al., 1997; Ujiie et al., 2004) and elsewhere (e.g., Agar et al., 1989; Prior and Behrmann, 1990; Maltman, 1998; Vannucchi and Tobin, 2000). Results from this study confirm by direct observation many of the ideas put forth in these previous papers, in particular the importance of particle rearrangement and porosity loss in the generation of planar deformation features. By employing a large set of samples selected without specific reference to macroscopically observed deformation features, this study is able to confirm the widespread and common occurrence of preferred alignments in the clay and silt fractions of muds in the Nankai accretionary complex.

The findings of this study with regard to compaction and bioturbation that generate fabric anisotropies in early diagenesis apply broadly to the interpretation of mudrock fabrics in a variety of depositional settings.

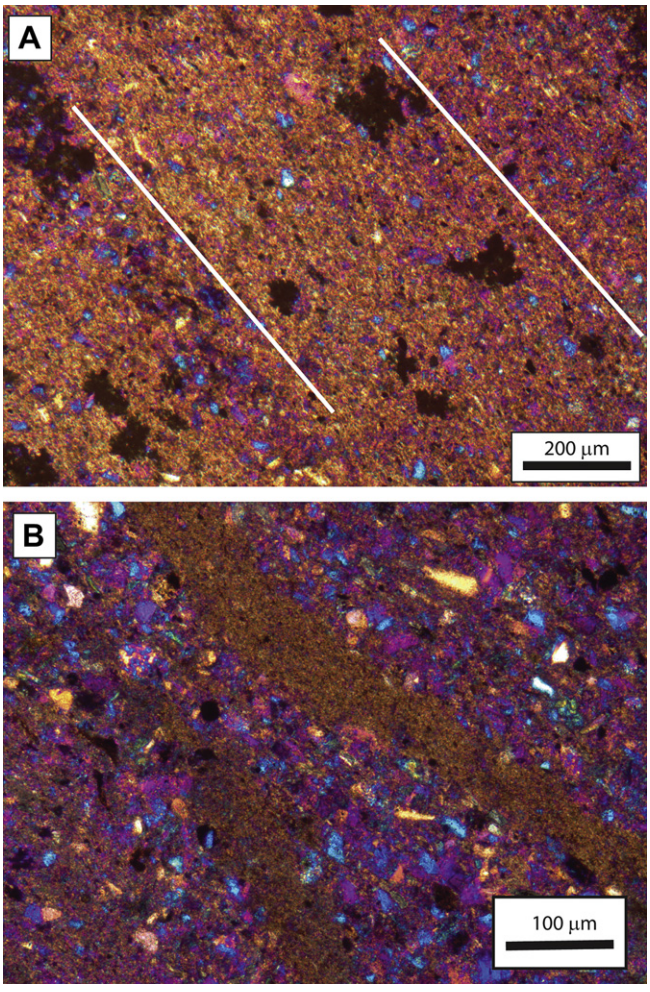

Fig. 3. Bed-parallel phyllosilicate alignment. All in cross-polarized transmitted light using a full-wave plate. A) Strong alignment of phyllosilicates parallel to bedding (trace of bedding indicated by white lines) results in a strong and pervasive yellow or blue coloration when the bedding is rotated at approximately 45° to the plane of polarization when using a full-wave (gypsum) plate. Sample C0006E-20X-3, 50 cm. B) Contrasting degrees of phyllosilicate alignment, as revealed by the color patterns seen using the full-wave plate, in clay-rich layers (distinctly yellow) and adjoining siltier layers (more random coloration). Sample C0004D-41R-1, 22 cm.

4.1. Compaction

Fabric anisotropy related to uniaxial shortening by compaction has been documented previously in the Nankai prism (Behrmann and Kopf, 1993; Morgan and Karig, 1993). In general, orientation of detrital phyllosilicates at deposition is believed to be highly random (Bowles et al., 1969; O'Brien and Slatt, 1990; Bennett et al., 1991). Because a high degree of bedding-parallel preferred orientation is observed in the shallowest samples in this study, it appears that random alignments, if present at deposition, have been markedly reorganized by early diagenesis. Disruption of bedding-parallel alignment by biogenic features confirms that layer-parallel fabric developed initially at a depth accessible to burrowing organisms. Alternatively, this bed-parallel fabric could have been developed by burial compaction at some depth and the re-exposed to near-surface bioturbation by some mechanism of sediment erosion on the slope.

4.2. Bioturbation

In previous study of fabric development in the Nankai accretionary prism the possible role of bioturbation in limiting development of preferred orientation was suggested by Morgan and Karig (1993). Results from our study make it clear that biogenic processes add complexity and considerable local heterogeneity to overall particle alignments. Bioturbation may generally act to disrupt preferred alignments (O'Brien, 1987), but may also act to create local regions of very strong alignments by active compaction of clays into burrow walls and linings.

It is difficult to prove conclusively that the generalized blotchy fabrics are biogenic. An alternative origin might be soft sediment deformation by slumping, however no larger-scale features (e.g., distorted bedding) could be connected to this fabric using observations at the thin section scale. In any case, it is clear that this fabric disrupts bedding-parallel alignment and therefore must post-date it.

4.3. Localized deformation features: mechanical aspects

Development of planar deformation bands, also appearing in some of the shallowest samples examined, must be seen in the context of the associated compactional and biogenic processes of particle alignment. Deformation bands cannot necessarily be modeled as arising within an assemblage of randomly arranged particles. Similarly, bulk measures of particle anisotropy, such as X-ray texture goniometry, must be interpreted in the context of the various modalities of preferred orientations that co-exist at the micro-scale.

Deformation bands in these muds arise largely from the development of preferred orientation of platy particles of both clay- and silt-size and concomitant loss of inter-particle primary porosity. Thus, they contain a true compaction component. At the micro-

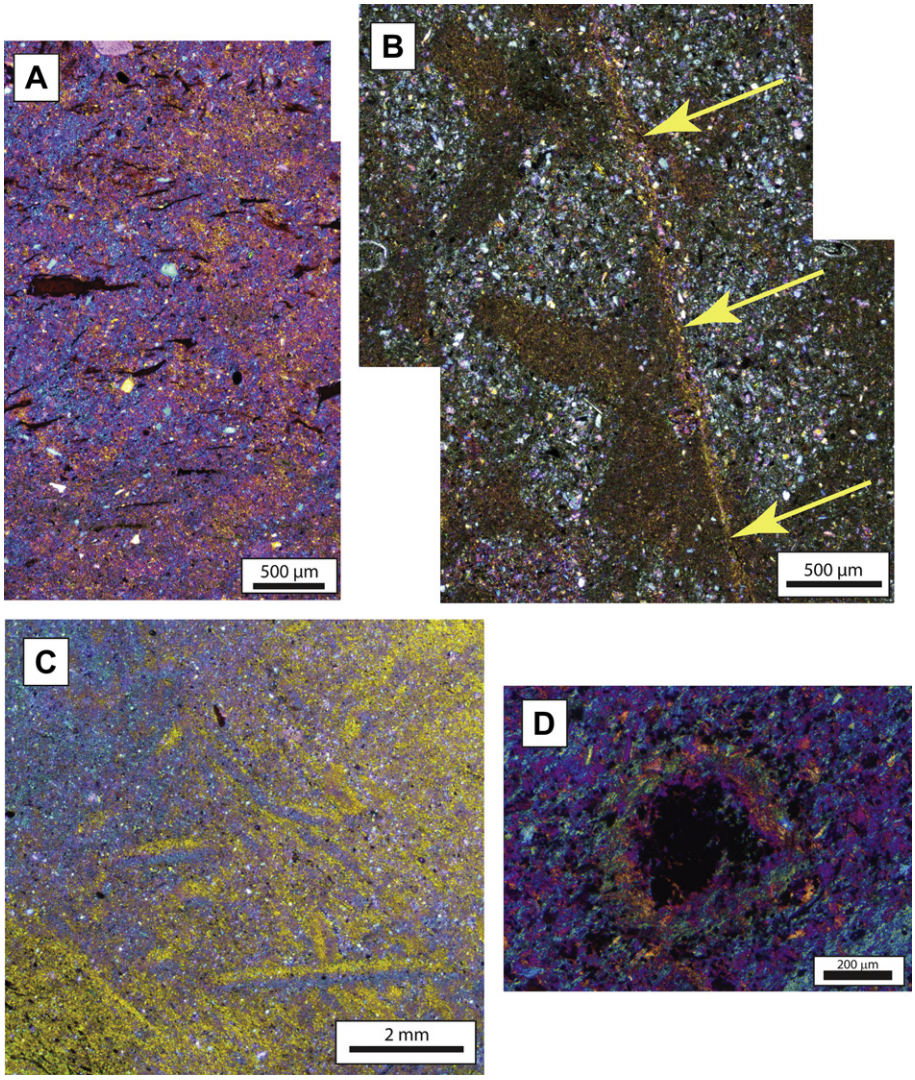

Fig. 4. Biogenically-induced alignments. All in cross-polarized transmitted light using a full-wave plate. A) Blotchy burrow mottling that is evident as regions of contrasting (blue and yellow) phyllosilicate alignment. Trace of bedding is horizontal. Sample C0006F-14R-1, 111 cm. B) Discrete clay-filled burrows (yellow-brown) filled with clay having a uniform alignment. Burrows (possible *Physcosiphon* isp.) are cut by a high-angle planar deformation structure. (yellow arrows). Sample C0006E-49X-2, 13 cm. C) Small criss-crossing tubular burrows filled or lined with highly oriented phyllosilicates. Sample C0007D-25R-3, 20 cm. D) Pyrite-filled tubular burrow lined with concentrically aligned clays. Sample C0004C-9H-5, 73 cm.

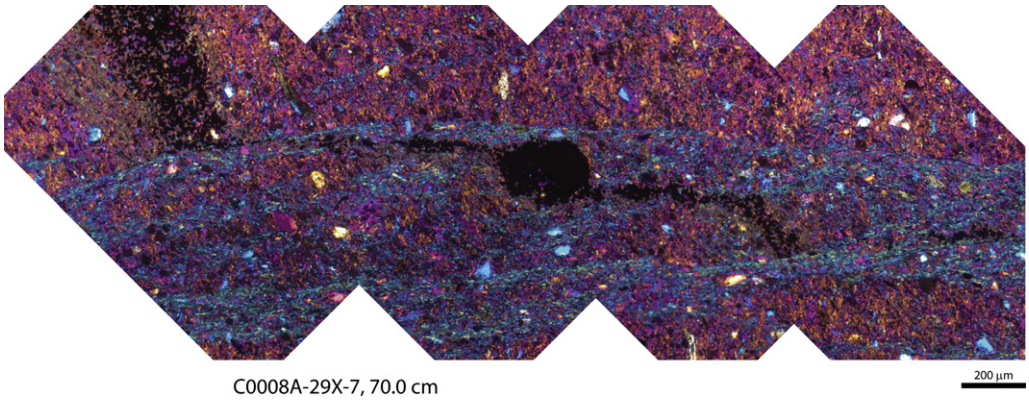

Fig. 5. Set of planar deformation bands (blue) that have displaced a pyrite-filled burrow. Shearing has distributed framboids (black) from the burrow several mm along the bands. Sample C0008A-29x-7, 70 cm. Cross-polarized transmitted light using a full-wave plate.

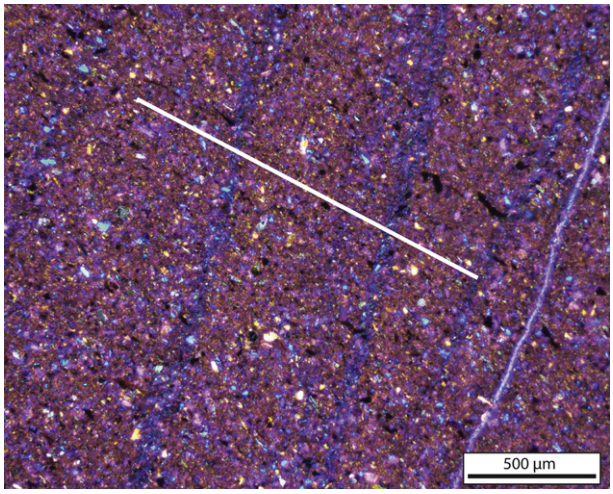

Fig. 6. Typical appearance of smaller bands (blue), developed in compaction-oriented sediment (yellow). White line indicate approximate plane of bedding. Sample C0008E-38X-CC, 23 cm. Cross-polarized transmitted light using a full-wave plate.

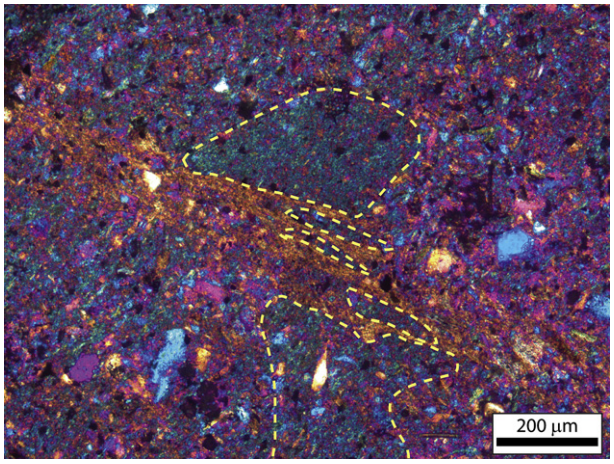

Fig. 7. Deformation band (yellow) showing a complex anastomosing form that surrounds pods of mud sheared from a burrow (yellow outlines).

scale, offset of 100s of microns are evident along some bands, indicating that they are not only compactional features but also small faults.

The approximately 5 percent porosity loss obtained from the high-resolution FE-SEM image of the Ar-milled surface matches well the 1 to 6 percent porosity loss in deformation bands at the toe of the prism determined from CT-density (Ujiie et al., 2004). Total measured porosities in the bulk sediment (Kinoshita et al., 2009) are far higher (generally between 45 and 60 percent at the depth of the sample imaged in Fig. 11) than the 8.6 percent observed in the FE-SEM image because the dominant pore population is <2 µm in diameter and cannot be measured accurately at the magnification employed. The match between our point-counted values for porosity loss and the values obtained from CT-density (a small-volume bulk method) suggests that loss of the larger-size pores is the dominant process and that additional loss of smaller-size pores may not make up a significant portion of the total porosity loss during band formation.

The observed BSE brightness of the bands also supports the notion that loss of intergranular pores may be a persistent feature of deformation bands in mudrocks. This contrasts with the situation in sandstones in which bands do not display a highly consistent

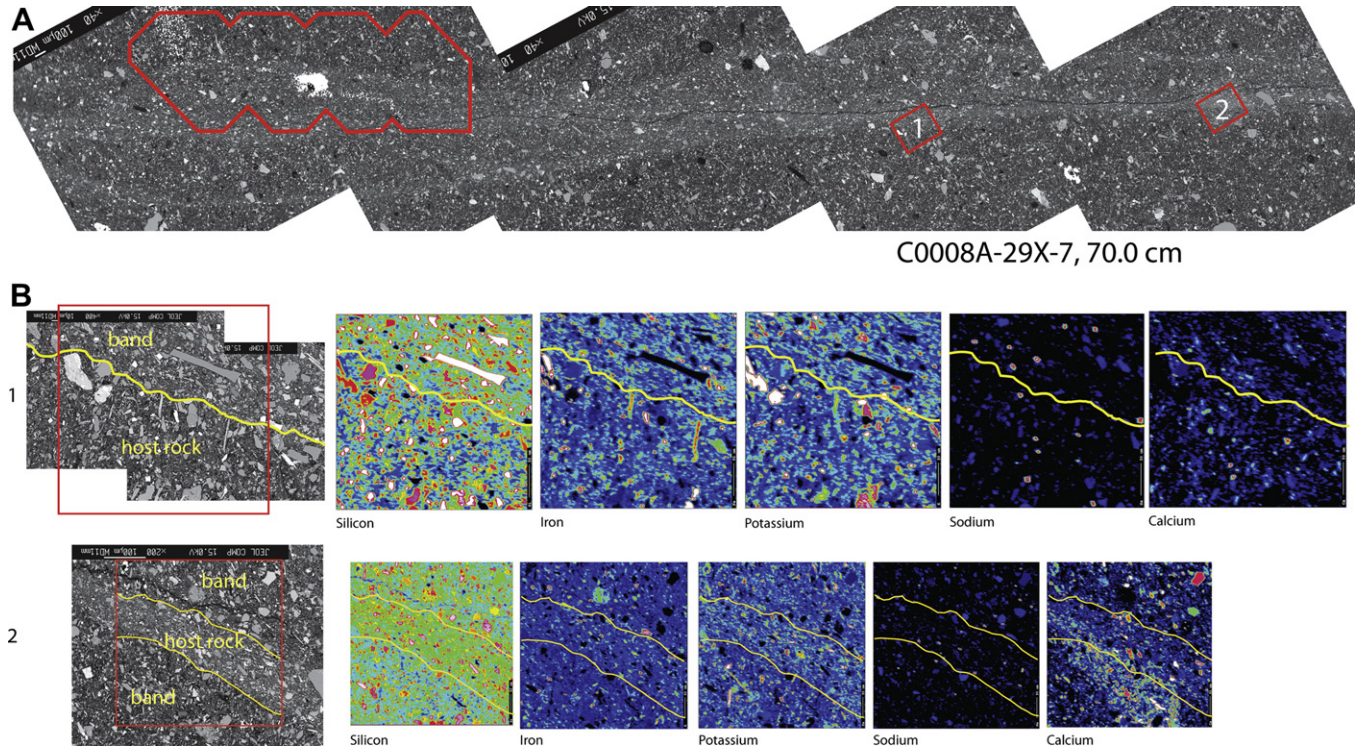

Fig. 8. Upper image (A) is a BSE mosaic of a band in sample C0008-29X-7, 70 cm. Outlined region on the left corresponds to the region of the light microscope image shown in FIG. 5. Pyrite is indicated by the brightest BSE intensity. Regions indicated by the smaller red boxes (B), labeled 1 and 2 on this upper image, correspond to the higher-magnification BSE images and associated X-ray maps marked 1 and 2 below. Among the X-ray maps only the Si-maps show a consistent higher concentration within the band. A subtle difference in K (higher in the band) is seen in map set 2, but not in map set 1. A distinct region of higher Ca-intensity is seen in map set 2, but it does not relate to the boundaries of the band and host rock.

Table 3
Summary of particle properties.

Sample	C0004D-53R-1, 72 cm		C0006E-21X-8, 58 cm		C0006E-27X-8, 6 cm	
	Host[c]	Band[c]	Host[d]	Band[d]	Host[d]	Band[d]
silt content (%)	28.1	18.1	28.3	23.8	28.7	22.0
relative orientation	78.8	61.7	82.3	106.4	97.0	99.4
length (μm)	6.8	5.6	5.9	6.3	7.3	5.0
width (μm)	3.3	2.6	3.0	3.1	3.9	3.0
mean grain size[a] (μm)	4.3	3.5	3.8	4.1	4.9	3.6
median grain size[a] (μm)	3.1	3.0	3.1	3.2	3.9	3.0
average size of coarsest 10%[a] (μm)	14.2	7.8	11.3	10.8	13.9	6.7
D[b]	1.9	2.5	2.0	2.1	1.8	2.2

[a] equivalent circular diameter.
[b] 2D fractal dimension.
[c] measurement determined from a single image at 1000x
[d] measurement determined from 3 1000x images.

pattern of increase or decrease of intergranular volume (IGV) compared to surrounding host rocks (Milliken et al., 2005; Eichhubl et al., this issue).

Evidence for particle comminution in mudrock bands is uncertain, as previously noted in other studies (Karig and Lundberg, 1990; Byrne et al., 1993). Assessing textural differences between bands and host rocks is a challenge. Given the prominent thin-section scale textural heterogeneity (Fig. 2D), materials of contrasting texture and composition can be brought into juxtaposition by the small-scale shear that accompanies band development, entirely apart from any textural modification of the sediment associated with band formation. A second challenge relates to the high magnifications that must be used to clearly image the particles. The necessarily small areas imaged at these high magnifications may not be representative of the larger-scale texture. Nonetheless, data for this study suggest subtle degrees of particle-size reduction within the silt fraction during band formation, especially within the coarser range of silt-size particles.

Of the three samples examined for particle size, one clearly has evidence for particle-size reduction across most of the size range examined, one has convincing evidence for the comminution of coarser-grained particles, and the third has no convincing evidence for a size contrast between the band and the host rock (Fig. 10). Possibly, the degree of particle-size reduction increases through a band's developmental history, and different bands will therefore manifest differing degrees of particle comminution. A more robust determination of textural differences between bands and host rocks will require a more extensive data set utilizing a larger number of image fields for both bands and host rocks.

Cataclasis is known from unconsolidated materials (e.g., Cashman and Cashman, 2000; Rawling and Goodwin, 2003), including those in forearcs (e.g., Lucas and Moore, 1986), but in general has been described as affecting mostly the sand-size fraction and as being generally more pronounced in coarser sand fractions (Chuhan et al., 2002; Makowitz and Milliken, 2003; Karner et al., 2005; Milliken et al., 2005; Eichhubl et al., this issue). In sandstones this style of localized deformation leads to modification of the pore system, as primary intergranular porosity is exchanged for intragranular porosity (Milliken et al., 2005; Eichhubl et al., this issue), and concomitant reduction of both particle size and pore size leads to lowering of permeability (Antonellini and Aydin, 1994). The lack of clearly defined particle comminution in the mudrock deformation bands described here may reflect the role of high porosity and the low degree of lithification in allowing the development of bands through particle rotation rather than particle breakage.

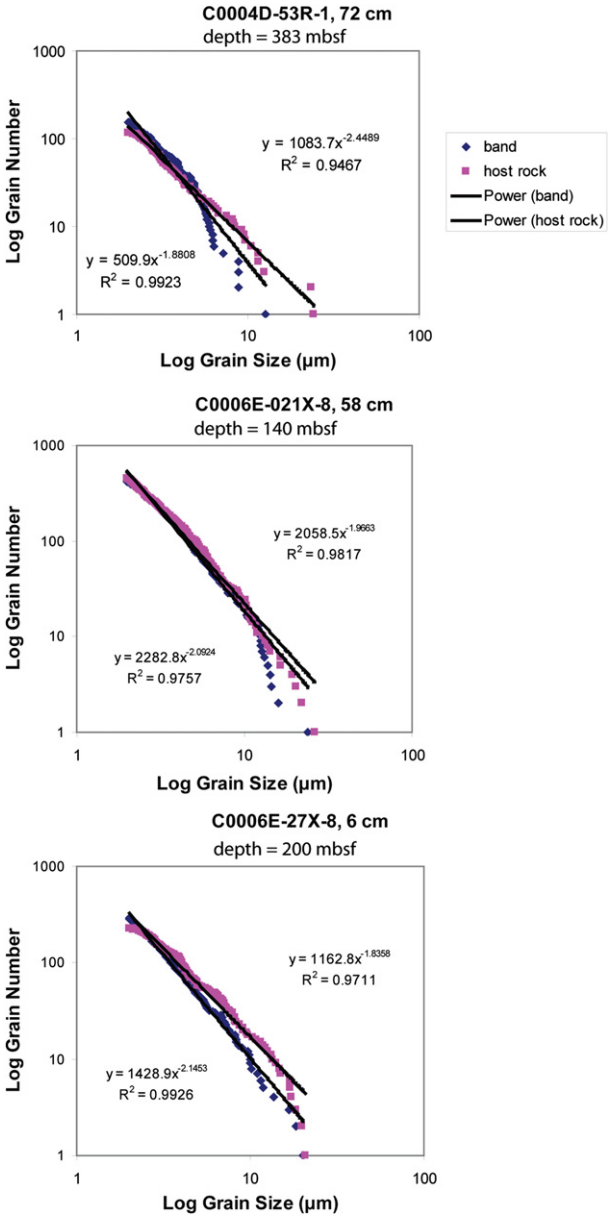

Fig. 9. Particle size distributions for the silt fraction in bands and corresponding host rocks. Only sample C0006E-27X-8, 6 cm shows a consistently finer population across most of the size range. Equations displayed on the lower left size of the plots are for the bands; those above the curves are for the host rocks. Bands generally display a fractal dimension (D in Table 3) somewhat higher than the host rocks.

4.4. Localized deformation features: chemical aspects

The general lack of elemental contrast between bands and host rocks is similar to the results reported by Byrne et al. (1993), based on energy-dispersive spectroscopy (EDS) transects across bands and adjacent host rocks. Byrne et al. observed only a localized increase in Fe. Caution must be exercised in interpretation of elemental change at band/host rock boundaries because, as with textural heterogeneity, materials of contrasting composition can be juxtaposed as a consequence of shear, as seen in the case of the pyrite from the sheared burrow in Figs. 5 and 8. The calcite-rich patch evident in the Ca-map in X-ray map set 2 (Fig. 8) shows an example of the primary compositional heterogeneity that is unrelated to the formation of the deformation band. Had the band cut

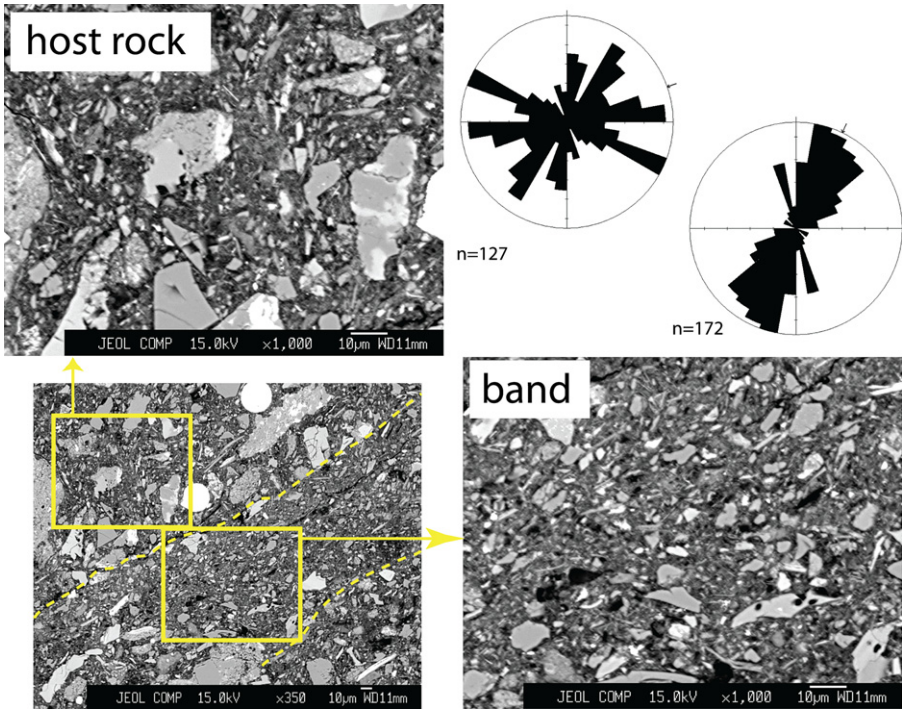

Fig. 10. Methodology and results of silt orientation measurements for Sample C0004D-53R-1m 72 cm. Images were obtained from within the band and host rock. All particles > 2 μm within each image were circumscribed with a digital pen and the objects thus created were analyzed using JMicrovision (Roduit, 2008). Relative orientations of the long-axes of these particle populations are shown in the rose diagrams.

through this region it might have given the appearance of either a higher or lower Ca-concentration in the band.

Illitization of smectite is not expected at the low temperatures of these sediments (<10 °C in the deepest samples; Kinoshita et al., 2009). The increase in Si (opposite to what is expected for illitization, e.g., Milliken, 2004 and references therein) and the lack of K increase observed in the bands confirm that illitization is not active in band development. The simplest explanation of Si-increase is porosity reduction, whereby the electron beam intersects more mineral matter, generating a stronger signal for this major element in the bands than in the surrounding host rock. Some degree of simple smectite dehydration during band formation as a consequence of localized pressure effects (e.g., Fitts et al., 1996) cannot be ruled out, however.

In sandstones, cement nucleation on surfaces created during deformational grain crushing creates patterns of enhanced cementation within deformation bands as compared to the host rocks (Milliken et al., 2005; Eichhubl et al., this issue). The lesser degree of particle comminution observed in the mudrock bands may ultimately lessen the localized chemical contrasts between bands and host rocks, even under thermal conditions more conducive to mineral reaction and precipitation.

4.5. Broader implications for mudrock pore systems

Direct observations of mudrock pores at high resolution in samples prepared in a way that minimizes mechanical damage are sparse in the published literature. The intergranular pores observed

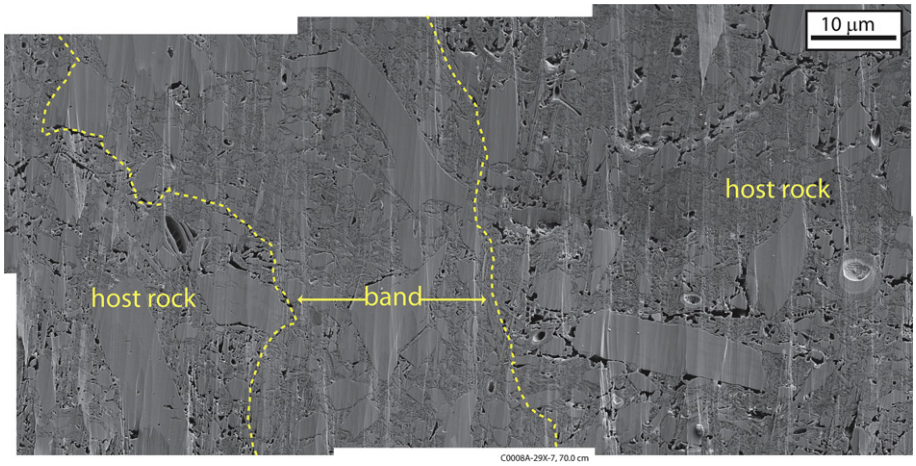

Fig. 11. High-resolution secondary electron image mosaic of an Ar-ion milled surface. The boundary between the deformation band and host rock is interpreted based upon a close examination of the fabric, including both particle orientations and porosity. Sample C0008A-29x-7, 70 cm.

here are very similar in form, distribution, and size to the ones reported by Desbois et al. (2009) using a related high-resolution imaging approach for the shallowly buried Oligocene Boom Clay in Belgium. In contrast, the pores observed here are far larger than organic-matter associated secondary pores imaged using FE-SEM in profoundly altered Paleozoic gas shales (Loucks et al., 2009). The dominance of intergranular pores in the relatively young, shallowly buried, and cool mudrocks studied here shows by contrast to the results of Loucks et al. (2009) that mudrock pore systems evolve dramatically in both volume and character as diagenesis progresses.

5. Conclusions

1. Early, pre-lithification diagenesis at the Expedition 316 sites on the Nankai accretionary complex entails development of small-scale fabric anisotropy in response to dominantly mechanical processes.
2. Compaction, burrowing, and localized planar deformation features all impose fabric modifications during the early stages of burial.
3. Relatively homogeneous compactional fabric alignments and more localized fabric anisotropies related to biogenic processes are nearly ubiquitous. Planar deformation fabrics are less abundant, but are still widely distributed.
4. The planar deformation bands observed in this study have a quantifiable compactional component and display visible loss of larger, micro-scale pores and development of preferred alignments of clay-size and silt-size particles.
5. Particle comminution and chemical modification are less-certain features of band development in these mudrocks.

Acknowledgments

This research used samples and data provided by the Integrated Ocean Drilling Program (IODP). Support for the project was provided by a grant to KLM from the Consortium for Ocean Leadership for Expedition 316 post-cruise research. The Jackson School of Geosciences is acknowledged for research support to RMR. KLM thanks Tim Byrne, Nick Hayman, and Ruarri-Day Stirrat for discussions and encouragement. The Expedition 316 Science Party and particularly sedimentologists, Michael Strasser, Uisdean Nicholson, and Chris Fergusson, are acknowledged for help with sampling and unfailing cheerfulness while describing many meters of mud. We thank Sean Gulick for providing the cross-section shown in Fig. 1. The manuscript benefited from the constructive review efforts of Andre Huepers, Diane Moore, Peter Vrolijk, and Joe Macquaker. Publication authorized by the Director, Bureau of Economic Geology.

References

Agar, S.M., Prior, D.J., Behrmann, J.H., 1989. Back-scattered electron imagery of the tectonic fabrics of some fine-grained sediments: implications for fabric nomenclature and deformation processes. Geology 17, 901–904.

Antonellini, M., Aydin, A., 1994. Effect of faulting on fluid flow in porous sandstones: petrophysical properties. American Association of Petroleum Geologists Bulletin 78, 355–377.

Behrmann, J.H., Kopf, A., et al., 1993. Textures and microfabrics in fine-grained muds and mudstones from site 808 nankai accretionary prism. 131. ODP. In: Hill, L.A., Taira, A., Firth, J.V. (Eds.), Proceedings of the Ocean Drilling Program, Scientific Results, pp. 46–56.

Bennett, R.H., O'Brien, N.R., Hulbert, M.H., 1991. Determinants of clay and shale microfabric signatures: processes and mechanisms. In: Bennett, R.H., O'Brien, N.R., Hulbert, M.H. (Eds.), Microstructure of Fine-grained Sediments. Springer-Verlag, New York, pp. 5–32.

Bowles, F.A., Bryant, W.R., Wallin, C., 1969. Microstructure of unconsolidated and consolidated marine sediments. Journal of Sedimentary Petrology 39, 1546–1551.

Byrne, T., Maltman, A., Stephenson, E., Soh, W., Knipe, R., et al., 1993. Deformation structures and fluid flow in the toe region of the nankai accretionary prism. 131. ODP. In: Hill, L.A., Taira, A., Firth, J.V. (Eds.), Proceedings of the Ocean Drilling Program, Scientific Results, pp. 83–101.

Cashman, S., Cashman, K., 2000. Cataclasis and deformation-band formation in unconsolidated marine terrace sand, Humboldt County California. Geology 28, 111–114.

Chuhan, F.A., Kjeldstad, A., Bjørlykke, K., Høeg, K., 2002. Porosity loss in sand by grain crushing–experimental evidence and relevance to reservoir quality. Marine and Petroleum Geology 19, 39–53.

Curtis, C.D., Lipshie, S.R., Oertel, G., Pearson, M.J., 1980. Clay orientation in some upper carboniferous mudrocks, its relationship to quartz content and some inferences about fissility, porosity and compactional history. Sedimentology 27, 333–339.

Day-Stirrat, R.J., Dutton, S.P., Milliken, K.L., Loucks, R.G., Aplin, A.C., Hillier, S., van der Pluijm, B.A., 2010. Diagenesis, phyllosilicate anisotropy, and physical properties in two fine-grained slope fan complexes; Texas Gulf Coast and Northern North Sea. Sedimentary Geology 208, 27–35.

Desbois, G., Urai, J.L., Kukla, P.A., 2009. Morphology of the pore space in claystones–evidence from BIB/FIB ion beam sectioning and cryo-SEM observations. eEarth Discussions 4, 1–19.

Eichhubl, P., Hooker, J.N. and Laubach, S.E., Pure and shear-enhanced compaction bands in Aztec Sandstone. Journal of Structural Geology this issue.

Fitts, T.G., Brown, K.M., Tryon, M.D., Anonymous, 1996. Gradual vs instantaneous dewatering of smectites; experimental data and implications for physical properties of smectite-rich sediments in nature. Geological Society of America 28 (7), 89. Abstracts with Programs.

Karig, D.E., Lundberg, N., 1990. Deformation bands from the toe of the nankai accretionary prism. Journal of Geophysical Research 95, 9099–9109.

Karner, S.L., Chester, J.S., Chester, F.M., Kronenberg, A.K., Hajash, A., 2005. Laboratory deformation of granular quartz sand: implications for the burial of clastic rocks. American Association of Petroleum Geologists Bulletin 89, 603–625.

Kinoshita, M., Tobin, H., Ashi, J., Kimura, G., Lallemant, S., Screaton, E.J., Curewitz, D., Masago, H., Moe, K.T., Scientists, E., 2009. NantroSEIZE Stage 1: Investigations of Seismogenesis, Nankai Trough, Japan. Integrated Ocean Drilling Program Management International, Inc, Washington, DC.

Laubach, S.E., 1997. A method to detect natural fracture strike in sandstone. American Association of Petroleum Geologists Bulletin 81, 604–623.

Laubach, S. E. Eichhubl, P., Hilgers, C. Lander, R.H., 2010, Structural diagenesis. this issue.

Lewis, J.C., Byrne, T., Prior, D.J., 1997. Small faults and kink bands in the Nankai accretionary complex: textural observations from site 808 of ODP leg 131. The Island Arc 6, 183–196.

Loucks, R.G., Reed, R.M., Ruppel, S.C., Jarvie, D.M., 2009. Morphology, genesis, and distribution of nanometer-scale pores in mudstones of the Mississippian Barnett Shale. Journal of Sedimentary Research 79, 848–861.

Lucas, S.E., Moore, J.C., 1986. Cataclastic deformation in accretionary wedges: deep sea drilling project leg 66, southern Mexico, and on-land examples from Barbados and Kodiak Islands. Memoir 166. In: Moore, C. (Ed.), Structural Fabric in Deep Sea Drilling Project Cores from Forearcs. Geological Society of America, pp. 121–135.

Macquaker, J.H.S., Adams, A.E., 2003. Maximizing information from fine-grained sedimentary rocks: an inclusive nomenclature for mudstones. Journal of Sedimentary Research 73, 735–744.

Makowitz, A., Milliken, K.L., 2003. Quantification of brittle deformation in burial compaction, Frio and Mt. Simon sandstones. Journal of Sedimentary Petrology 73, 999–1013.

Maltman, A., 1998. Deformation structures from the toes of active accretionary prisms. Journal of the Geological Society of London 155, 305–343.

Maltman, A., Byrne, T., Karig, D.E., Lallemant, S., 1993. Deformation at the toe of an active accretionary prism: synopsis of results from ODP Leg 131, Nankai, SW Japan. Journal of Structural Geology 15, 949–964.

Milliken, K.L., 1994. The widespread occurrence of healed microfractures in siliciclastic rocks: evidence from scanned cathodoluminescence imaging. In: Nelson, P.A., Laubach, S.E. (Eds.), North American Rock Mechanics Symposium. Balkema, Austin, Texas, pp. 825–832.

Milliken, K.L., et al., 2003. Diagenesis. In: Middleton, G.V., Church, M.J., Coniglio, M. (Eds.), Encyclopedia of Sediments and Sedimentary Rocks. Kluwer Academic Publishers, Dordrecht, pp. 214–219.

Milliken, K.L., 2004. Late diagenesis and mass transfer in sandstone-shale sequences. In: Mackenzie, F.T. (Ed.), Sediments, Diagenesis, and Sedimentary Rocks. Treatise on Geochemistry 7. Elsevier-Pergamon, Oxford, pp. 159–190.

Milliken, K.L., Laubach, S.E., et al., 2000. Brittle deformation in sandstone diagenesis as revealed by scanned cathodoluminescence imaging with application to characterization of fractured reservoirs. In: Pagel, M., Barbin, V., Blanc, P. (Eds.), Cathodoluminescence in Geosciences. Springer, Berlin, pp. 225–243.

Milliken, K.L., Reed, R.M., Laubach, S.E., 2005. Quantifying compaction and cementation in deformation bands in porous sandstones. In: AAPG Memoir 85. American Association of Petroleum Geologists, Tulsa, OK, United States, pp. 237–249.

Moore, G.F., Park, J.-O., Bangs, N.L., Gulick, S.P., Tobin, H., Nakamura, Y., Sato, S., Tsuiji, T., Yoro, T., Tanaka, H., Urakai, S., Kido, Y., Kuramoto, S., Taira, A., et al., 2009. Structural and seismic stratigraphic framework of the NanTroSEIZE State 1 Transect: kumano 3D seismic survey. In: Kinoshita, M., Tobin, H., Ashi, J. (Eds.), Proceedings of the Integrated Ocean Drilling Program Expeditions 314/315/316.

Integrated Ocean Drilling Program Management International, Washington, D.C. doi:10.2204/iodp.proc.314315316.102.2009.
Morgan, J.K., Karig, D.E., et al., 1993. Ductile strains in clay-rich sediments from hole 808C: preliminary results using X-ray pole figure goniometry. In: Hill, L.A., Taira, A., Firth, J.V. (Eds.), Proceedings of the Ocean Drilling Program, Scientific Results, 131, pp. 141–153.
O'Brien, N.R., 1987. The effects of bioturbation on the fabric of shale. Journal of Sedimentary Petrology 57, 449–455. Society of Economic Paleontologists and Mineralogists: Tulsa, OK, United States.
O'Brien, N.R., Slatt, R.M., 1990. Argillaceous Rock Atlas. Springer-Verlag, New York.
Oertel, G., 1983. The relationship of strain and preferred orientation of phyllosilicate grains in rocks-a review. Tectonophysics 100, 413–447.
Prior, D.J., Behrmann, J.H., 1990. Thrust-related mudstone fabrics from the Barbados forearc: a backscattered scanning electron microscope study. Journal of Geophysical Research 95, 9055–9067.
Rawling, G.C., Goodwin, L.B., 2003. Cataclasis and particulate flow in faulted, poorly lithified sediments. Journal of Structural Geology 25, 317–331.
Roduit, N., 2008. JMICROVISION: Image Analysis Toolbox for Measuring and Quantifying Components of High-definition Images.
Screaton, E.J., Kimura, G., Curewitz, D., Moore, G., IODP Expeditions 314, 316 Scientific Parties., 2009. Interactions between deformation and fluids in the frontal thrust region of the NanTroSEIZE transect offshore the Kii Peninsula, Japan: Results from IODP Expedition 316 Sites C0006 and C0007. Geochemistry Geophysics Geosystems. submitted for publication. 10, 2009. doi:10.1029/2009GC002713 Q0AD01.
Strasser, M., Moore, G.F., Kimura, G., Kitamura, Y., Kopf, A.J., Lallemant, S., Park, J.-O., Screaton, E.J., Su, X., Underwood, M.B., Zhao, X., 2009. Origin and evolution of a splay fault in the nankai accretionary wedge. Nature Geoscience 2 (9), 648–652.
Ujiie, K., Maltman, A., Sanchez-Gomez, M., Tobin, H., 2004. Deformation bands in argillaceous sediments at the toe of the nankai accretionary prism, southwest Japan. Journal of Structural Geology 26, 221–231.
Vannucchi, P., Tobin, H., 2000. Deformation structures and implications for fluid flow at the Costa Rica convergent margin, ODP Sites 1040 and 1043, Leg 170. Journal of Structural Geology 22, 1087–1103.